Technical Note

Estimation of Elastic Compliance Matrix of Rock Mass Containing Penny-Shaped Fractures

Jianping Yang[1]; Weizhong Chen[2]; Diansen Yang[3]; and Guojun Wu[4]

Abstract: In geotechnical engineering, fracture fillings or rough fracture surfaces often resist deformation and enhance the equivalent elastic moduli of fractured rock masses. In this study, the normal stiffness and shear stiffness of penny-shaped fractures were incorporated into the open-fracture model to account for the normal and shear resistance of fracture fillings. Based on the derived displacements of a penny-shaped fracture incorporating fracture stiffness, the compliance matrices of two special fracture distributions, the parallel distribution and random distribution, were obtained. The analytical results show that three-dimensional (3D) models predicted larger elastic moduli than the corresponding two-dimensional (2D) models, and models considering fracture stiffness predicted larger elastic moduli than the open-fracture models. Elastic moduli were underestimated by 30–40% in a 2D open-fracture model compared with the result of the corresponding 3D model. The difference in elastic moduli between 2D and 3D models was found to decrease when the fracture stiffness was considered. In the present study, the difference was less than 15%. **DOI:** 10.1061/(ASCE)GM.1943-5622.0001385. *© 2019 American Society of Civil Engineers.*

Author keywords: Rock mass; Compliance tensor; Compliance matrix; Penny-shaped fracture; Stiffness.

Introduction

The elastic compliance matrix of a fractured rock mass is an important parameter in the stability analysis of civil and mining structures built in or on rock masses. Several methods are commonly used to estimate the elastic moduli of fractured rock masses, including in situ tests (Bieniawski 1978), empirical methods based on rock-mass classification (Palmstrøm 1996; Barton 2002; Zhang and Einstein 2004; Hoek and Diederichs 2006), numerical methods based on explicit fracture representation (Kulatilake et al. 1993; Min and Jing 2003; Esmaieli et al. 2010; Yang et al. 2014; Gutierrez and Youn 2015; Farahmand et al. 2018), and analytical methods (Amadei and Goodman 1981; Cai and Horii 1992; Hu and Huang 1993; Huang et al. 1995; Li 2001; Wang and Huang 2009; Agharazi et al. 2012; Yang et al. 2016, 2018). Analytical solutions have the advantage of being compact, clear, and straightforward.

[1]Associate Professor, State Key Laboratory of Geomechanics and Geotechnical Engineering, Institute of Rock and Soil Mechanics, Chinese Academy of Science, Wuhan, Hubei 430071, China. Email: jpyang@whrsm.ac.cn

[2]Professor, State Key Laboratory of Geomechanics and Geotechnical Engineering, Institute of Rock and Soil Mechanics, Chinese Academy of Science, Wuhan, Hubei 430071, China; Professor, Research Centre of Geotechnical and Structural Engineering, Shandong Univ., Jinan, Shandong 250061, China (corresponding author). Email: wzchen@whrsm.ac.cn

[3]Professor, State Key Laboratory of Geomechanics and Geotechnical Engineering, Institute of Rock and Soil Mechanics, Chinese Academy of Science, Wuhan, Hubei 430071, China. Email: dsyang@whrsm.ac.cn

[4]Associate Professor, State Key Laboratory of Geomechanics and Geotechnical Engineering, Institute of Rock and Soil Mechanics, Chinese Academy of Science, Wuhan, Hubei 430071, China. Email: gjwu@whrsm.ac.cn

The equivalent elastic constants of fractured bodied are studied extensively in the framework of the energy-equivalence method or the strain-average method (Budiansky and O'Connell 1976; Horii and Nemat-Nasser 1983; Oda et al. 1984; Hudson 1994; Grechka 2005; Saenger et al. 2004; Takekawa et al. 2014). An important step in the process is to calculate the energy loss or the additional strain produced by a single isolated fracture, in which the fracture resistances are the key. The fracture resistances are treated in different ways in different fracture models:

1. For persistent fractures, the normal stiffness and shear stiffness of fractures are commonly set as finite values to represent the compressive and shear resistances (Amadei and Goodman 1981; Huang et al. 1995; Wang and Huang 2009; Agharazi et al. 2012).
2. For nonpersistent fractures, the fracture is mostly assumed to be liquid filled in geophysics, relating to the seismic characterization of the fractured reservoir (Bakulin et al. 2000; Berryman 2007; Hall and Wang 2012; Saxena and Mavko 2015), or is assumed to be a gas filled in geotechnics, where the fracture stiffness is zero (Budiansky and O'Connell 1976; Kemeny and Cook 1986).

The open-fracture model in geotechnics is suitable for fractures under tensional stress (Hu and Huang 1993) or stress sufficiently small so as not to produce contact between the opposite fracture surfaces (Budiansky and O'Connell 1976). For fractures under compression, closure effects and slip friction of fracture surfaces may cause load-induced anisotropy in elastic moduli, and the closed fracture, whose stiffness is infinitely great, is then taken into account (Horii and Nemat-Nasser 1983; Kachanov 1993).

Compared to the ideal situations in which the stiffness of nonpersistent fractures is zero or infinitely great, the normal stiffness and shear stiffness of nonpersistent fractures are finite values in practical engineering because of the mismatch of fracture surfaces and/or the fracture fillings, which may be naturally formed or manually produced during construction processes, such as grouting and shotcrete. Considering the finite stiffness of two-dimensional (2D) nonpersistent fractures, Yang et al. (2016) analytically studied the displacement jumps of fractures and the directional elastic moduli

of the fractured rock mass. Furthermore, the compliance matrices of rock masses containing 2D nonpersistent fractures were derived based on the energy-equivalence method and the strain-average method (Yang et al. 2018). However, these studies were limited to 2D rectilinear fractures and rock masses. For three-dimensional (3D) nonpersistent fractures and rock masses, the effects of fracture stiffness are still not included in the analytical estimation of equivalent compliance matrices.

In this article, the mean normal and shear displacements of a penny-shaped fracture considering fracture stiffness are first derived. Then, the general expressions of a compliance matrix for a rock mass containing penny-shaped fractures are obtained in the framework of the strain-average method. Compliance matrices of two special fracture distributions, the parallel and random distribution, are further derived. Finally, the errors of elastic moduli are estimated between the derived 3D fracture model, the 3D open-fracture model, and the corresponding 2D fracture models.

Displacement of Penny-Shaped Fractures Considering Fracture Stiffness

From the theory of linear-elastic fracture mechanics, the normal displacement of a penny-shaped fracture is given by Eq. (1) (Gross and Seelig 2006),

$$u = \frac{2(1 - v_0)\sigma_n}{\pi G_0}\sqrt{a^2 - r^2} \quad (1)$$

Eq. (1) is valid for open fractures. When the normal stiffness of a fracture is considered, the normal compliance is reduced because the stress σ_n in Eq. (1) is reduced to an effective value σ_e. So, for a penny-shaped fracture considering normal stiffness, the normal displacement is

$$u = \frac{2(1 - v_0)\sigma_e}{\pi G_0}\sqrt{a^2 - r^2} \quad (2)$$

where $\sigma_e = \sigma_n - \sigma_k$; $\sigma_k = 2K_n u$; and K_n = normal stiffness of the fracture.

From Eq. (2), it can be seen that the displacement along the fracture radius is complicated, and it is cumbersome to obtain the mean displacement, which will be used to estimate the compliance tensor of the rock mass. The displacement can be assumed to be uniform for a 2D rectilinear fracture when the fracture stiffness is considered (Yang et al. 2016). In this article, the displacement along the fracture radius is also assumed to be uniform for a 3D penny-shaped fracture. Thus, σ_k and σ_e are uniform from the equations $\sigma_k = 2K_n u$ and $\sigma_e = \sigma_n - \sigma_k$.

The mean displacement $\bar{u}$ of a fracture is estimated from Eq. (2) as

$$\bar{u} = \frac{1}{A}\int_A u \, dA = \frac{4(1 - v_0)a}{3\pi G_0} \cdot \sigma_e \quad (3)$$

Also,

$$\sigma_e = \sigma_n - \sigma_k = \sigma_n - 2K_n\bar{u} \quad (4)$$

Substituting Eq. (4) into Eq. (3), the mean normal displacement of a penny-shaped fracture considering normal stiffness can be obtained as

$$\bar{u} = B_1\sigma_n \quad (5)$$

where $B_1 = [4(1 - v_0)a]/[8K_n(1 - v_0)a + 3\pi G_0]$.

Following the same procedure, the mean shear displacement of a penny-shaped fracture considering shear stiffness is

$$\bar{v} = B_2\tau_s \quad (6)$$

where $B_2 = [8(1 - v_0)a]/[16K_s(1 - v_0)a + 3\pi G_0(2 - v_0)]$.

The mean displacements in Eqs. (5) and (6) reduce to the classic analytical results for an open fracture by setting the normal stiffness and shear stiffness to zero.

Compliance Matrix of Rock Mass Containing Penny-Shaped Fractures

For an elastic body containing fractures, the average strain tensor is related to the average stress tensor through an elastic compliance tensor D_{ijkl} as follows:

$$\varepsilon_{ij} = D_{ijkl}\sigma_{kl} \; (i,j,k,l = 1,2,3) \quad (7)$$

D_{ijkl} consists of two parts: the first M_{ijkl} depends on the elasticity of intact rock without any fractures, whereas the second C_{ijkl} represents the correction factor related to the existing fractures

$$D_{ijkl} = M_{ijkl} + C_{ijkl} \quad (8)$$

Using the divergence theorem, Horii and Nemat-Nasser (1983) proved that C_{ijkl} satisfies the following:

$$C_{ijkl}\sigma_{kl} = \frac{1}{V}\int_{2A^{(\text{all})}} \frac{1}{2}(u_i n_j + u_j n_i)dA \quad (9)$$

where V = total volume of the fractured body; $2A^{(\text{all})}$ = total surface area of all fractures (every fracture consists of two surfaces, each of which has an area A); $u_i, u_j \; (i,j = 1,2,3)$ are the components of a displacement vector; and n_i, n_j = components of a unit vector normal to fracture surfaces.

For each flat, penny-shaped fracture, n_i, n_j are constant along its surface. The contribution of each fracture on C_{ijkl} is derived by Oda et al. (1984) as

$$\frac{1}{2V}\int_{2A}(u_i n_j + u_j n_i)dA = \frac{A}{2V}(\delta_i n_j + \delta_j n_i) \quad (10)$$

where δ_i = mean displacement jump, defined by

$$\delta_i = \frac{1}{A}\int_{2A} u_i \, dS = 2\bar{u}_i \quad (11)$$

Thus, in a rock mass containing $m^{(V)}$ penny-shaped fractures, C_{ijkl} can be estimated by summing the contributions of all fractures inside volume V from Eq. (9), as follows:

$$C_{ijkl}\sigma_{kl} = \frac{A}{2V}\sum_{k=1}^{m^{(V)}}(\delta_i n_j + \delta_j n_i) \quad (12)$$

To express the term $\delta_i n_j + \delta_j n_i$ in Eq. (12), two coordinate systems are defined in Fig. 1. The local coordinate system (n, s, t) is defined on the fracture surface: n is normal to the fracture surface, and s and t are in-surface axes. The rotation matrix α is

used to translate $\delta_n, \delta_s, \delta_t(\delta_n = \delta_{1'}, \delta_s = \delta_{2'}, \delta_t = \delta_{3'}$ in the local coordinate system) to δ_i, δ_j $(i, j = 1, 2, 3)$ in the global coordinate system. The rotation matrix β is used to express

σ_n, τ_s, τ_t $(\sigma_n = \sigma_{1'1'}, \tau_s = \sigma_{1'2'}, \tau_t = \sigma_{1'3'})$ in Eqs. (5) and (6) from σ_{ij} in the global coordinate system. Thus, $\delta_i n_j + \delta_j n_i$ can be expressed as

$$
\begin{aligned}
\delta_i n_j + \delta_j n_i &= \alpha_{ik'}\delta_{k'} n_j + \alpha_{jl'}\delta_{l'} n_i = (\alpha_{i1'}\delta_{1'} + \alpha_{i2'}\delta_{2'} + \alpha_{i3'}\delta_{3'})n_j + (\alpha_{j1'}\delta_{1'} + \alpha_{j2'}\delta_{2'} + \alpha_{j3'}\delta_{3'})n_i \\
&= 2(B_1\alpha_{i1'}\sigma_{1'1'} + B_2\alpha_{i2'}\sigma_{1'2'} + B_2\alpha_{i3'}\sigma_{1'3'})n_j + 2(B_1\alpha_{j1'}\sigma_{1'1'} + B_2\alpha_{j2'}\sigma_{1'2'} + B_2\alpha_{j3'}\sigma_{1'3'})n_i \\
&= 2[B_1(\alpha_{i1'}n_j + \alpha_{j1'}n_i)\beta_{1'k}\beta_{1'l} + B_2(\alpha_{i2'}n_j + \alpha_{j2'}n_i)\beta_{1'k}\beta_{2'l} + B_2(\alpha_{i3'}n_j + \alpha_{j3'}n_i)\beta_{1'k}\beta_{3'l}]\sigma_{kl}
\end{aligned}
\tag{13}
$$

From Eqs. (12) and (13), the elastic compliance tensor for arbitrarily distributed penny-shaped fractures can be obtained.

Rock Masses Containing Sets of Penny-Shaped Fractures

Summation and Transformation of the Fracture Compliance Tensor

For rock masses containing several sets of fractures, the fracture compliance tensor [C_{ijkl} in Eq. (8)] can be determined by the summation of the compliance tensors for each fracture set (Fracture Set 1, Fracture Set 2, …, Fracture Set N) in the global coordinate system, as follows:

$$C_{ijkl} = C_{ijkl}^{set1} + ... + C_{ijkl}^{setN} \tag{14}$$

For each fracture set, the compliance tensor in the local coordinate system can be transferred to the global coordinate system. In

practical usage, the compliance tensor is often expressed as a 6×6 compliance matrix (S), as shown in Eq. (15). Accordingly, a 6×6 matrix [T in Eq. (16)] is introduced for the transformation of the compliance matrix between the global and local coordinate systems (Min and Jing 2003). The meanings of the symbols in T are given in Table 1. Eq. (17) shows the transformation formula, where S and S' are the compliance matrix in the global and local coordinate systems, respectively.

$$
\begin{Bmatrix} \varepsilon_{xx} \\ \varepsilon_{yy} \\ \varepsilon_{zz} \\ \varepsilon_{yz} \\ \varepsilon_{xz} \\ \varepsilon_{xy} \end{Bmatrix} = \begin{pmatrix} S_{11} & S_{12} & S_{13} & S_{14} & S_{15} & S_{16} \\ S_{21} & S_{22} & S_{23} & S_{24} & S_{25} & S_{26} \\ S_{31} & S_{32} & S_{33} & S_{34} & S_{35} & S_{36} \\ S_{41} & S_{42} & S_{43} & S_{44} & S_{45} & S_{46} \\ S_{51} & S_{52} & S_{53} & S_{54} & S_{55} & S_{56} \\ S_{61} & S_{62} & S_{63} & S_{64} & S_{65} & S_{66} \end{pmatrix} \begin{Bmatrix} \sigma_{xx} \\ \sigma_{yy} \\ \sigma_{zz} \\ \tau_{yz} \\ \tau_{xz} \\ \tau_{xy} \end{Bmatrix}
\tag{15}
$$

$$
T = \begin{pmatrix}
l_1^2 & m_1^2 & n_1^2 & 2m_1n_1 & 2n_1l_1 & 2l_1m_1 \\
l_2^2 & m_2^2 & n_2^2 & 2m_2n_2 & 2n_2l_2 & 2l_2m_2 \\
l_3^2 & m_3^2 & n_3^2 & 2m_3n_3 & 2n_3l_3 & 2l_3m_3 \\
l_2l_3 & m_2m_3 & n_2n_3 & m_2n_3 + n_2m_3 & n_2l_3 + l_2n_3 & l_2m_3 + m_2l_3 \\
l_3l_1 & m_3m_1 & n_3n_1 & m_3n_1 + n_3m_1 & n_3l_1 + l_3n_1 & l_3m_1 + m_3l_1 \\
l_1l_2 & m_1m_2 & n_1n_2 & m_1n_2 + n_1m_2 & n_1l_2 + l_1n_2 & l_1m_2 + m_1l_2
\end{pmatrix}
\tag{16}
$$

$$\mathbf{S} = \mathbf{TS'T}^{-1} \tag{17}$$

Elastic Compliance Matrix of One Set of Parallel Fractures

For one set of parallel penny-shaped fractures, the fracture compliance tensor (C_{ijkl}) can be obtained easily from Eqs. (12) and (13) by setting the local coordinate system (n, s, t) to coincide with the global coordinate system (x, y, z), as presented in Fig. 2. Furthermore, the fracture compliance matrix S can be obtained by comparing components of S from Eq. (15) and components of C_{ijkl} from its tensor form $\varepsilon_{ij} = C_{ijkl}\sigma_{kl}$. For one set of fractures, presented in Fig. 2, the results of S_{11}, S_{55}, and S_{66} are obtained and presented in Eqs. (18)–(20). The other components in S are zero. Thus, the fracture compliance

matrix for one set of penny-shaped fractures considering fracture stiffness is expressed in Eqs. (18)–(21).

$$S_{11} = C_{1111} = \frac{8\rho\pi(1-v_0)a^3}{8K_n(1-v_0)a + 3\pi G_0} \tag{18}$$

$$S_{55} = C_{1313} + C_{1331} = \frac{8\rho\pi(1-v_0)a^3}{16K_s(1-v_0)a + 3\pi G_0(2-v_0)} \tag{19}$$

$$S_{66} = C_{1212} + C_{1221} = \frac{8\rho\pi(1-v_0)a^3}{16K_s(1-v_0)a + 3\pi G_0(2-v_0)} \tag{20}$$

$$\mathbf{S_{parallel}} = \begin{pmatrix} \mathbf{S}_{11} & & & & & \\ & 0 & & & & \\ & & 0 & & & \\ & & & 0 & & \\ & & & & \mathbf{S}_{55} & \\ & & & & & \mathbf{S}_{66} \end{pmatrix} \qquad (21)$$

Eqs. (18)–(21) reduce to the result of open fractures by setting $K_n = K_s = 0$ (Kachanov 1993). For persistent fractures, Eqs. (18)–(21) reduce to the closed-form results of Amadei and Goodman (1981) by setting the fracture density as $\rho = \left[(L/d)/(\pi a^2 L)\right] = \left(1/\pi a^2 d\right)$ and the fracture radius a as infinitely large.

Comparison of Elastic Moduli of One Set of Fractures between 3D and 2D Models

First, consider parallel penny-shaped fractures of a given radius a (Fig. 2); the intersection of a penny-shaped fracture with the x,z cutting plane is a chord (2D fracture) of length $2a_{2D}$. Because the 3D fractures are uniformly distributed in space, the fractures close to the x,z cutting plane within a certain distance (in the special case as illustrated in Fig. 2, the distance is a) should intersect the cutting plane, and the distance r_d of the chord to the fracture center is uniformly distributed. Thus, the number of 3D fractures intersecting the cutting plane with the square L^2 is $2L^2 a\rho$, and the 2D fracture density (defined as the number of 2D fractures per square meter) can be obtained as

$$\rho_{2D} = 2L^2 a\rho / L^2 = 2a\rho \qquad (22)$$

where r_d is related to a_{2D} by the relation $a_{2D} = \sqrt{a^2 - r_d^2}$. The average half length of the chords $\langle a_{2D} \rangle$ is derived in Eq. (23), which is a special case of Berkowitz and Adler's (1998) result.
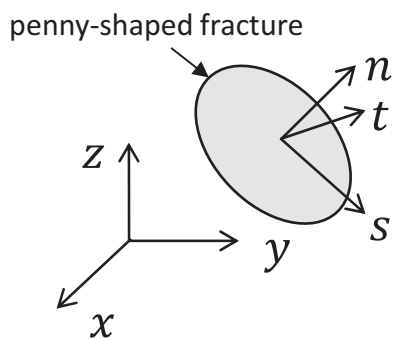
Fig. 1. Global coordinate system (x, y, z) and local coordinate system (n, s, t).

Table 1. Symbols for the directional cosines in rectangular x,y,z-axes and n,s,t-axes

Axis	Axis		
	x	y	z
n	l_1	l_2	l_3
s	m_1	m_2	m_3
t	n_1	n_2	n_3

$$\langle a_{2D} \rangle = \int_0^a \frac{\sqrt{a^2 - r_d^2}}{a} dr_d = \frac{\pi a}{4} \qquad (23)$$

Using Eqs. (22) and (23) and the compliance matrix of 2D non-persistent fractures (Yang et al. 2018), the compliance matrix of the corresponding 2D trace map can be estimated.

A case study was performed on a rock mass, and the parameters of the material are listed in Table 2. The obtained directional elastic moduli in the x,z-plane are plotted in Fig. 3. The elastic moduli of the 3D open-fracture model and the results of the corresponding 2D models are also plotted in Fig. 3 for comparison. The results show that the elastic modulus was equal to the value of intact rock in the orientation parallel to the fracture surface (z-axis) and decreased quickly when the orientation deviated from the z-axis. Compared with the open-fracture model, the proposed model considering fracture stiffness predicted larger elastic moduli, especially in the $\pi/4$ angular range around the fracture normal direction (x-axis; Fig. 3). The elastic moduli of the corresponding 2D models present a similar evolution to the 3D models, but the values of elastic moduli are smaller than those of the 3D models. The 2D open-fracture model underestimated the elastic moduli by 31% compared with the corresponding the 3D model. With consideration of the fracture stiffness, the underestimation percentage was 11%.

Rock Masses Containing Randomly Distributed Penny-Shaped Fractures

For randomly distributed penny-shaped fractures, the number of fractures (dN) having unit normal vectors oriented inside a small solid angle $d\Omega$ (Fig. 4) around $\mathbf{n}$ is $(V\rho/2\pi)d\Omega$. Thus, Eq. (10) becomes

$$\frac{A}{2V}(\delta_i n_j + \delta_j n_i)dN = \frac{\rho a^2}{4}(\delta_i n_j + \delta_j n_i)d\Omega \qquad (24)$$

Integrating Eq. (24) over $0 \leq \Omega/2 \leq 2\pi$, it becomes the right side of Eq. (9) because all fractures are taken into account. Using Eq. (13) results in
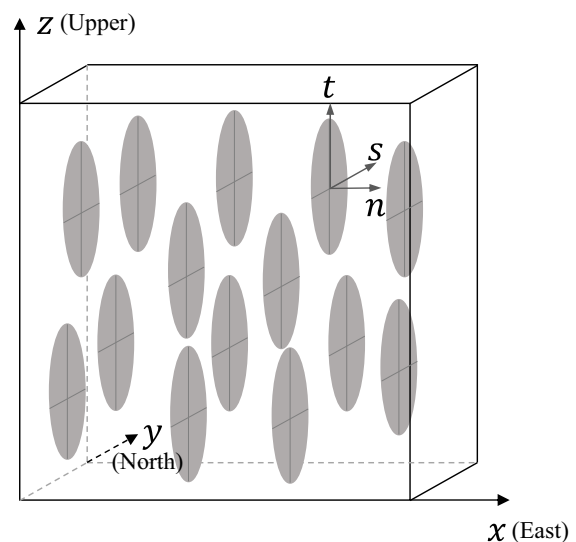
Fig. 2. Rock mass containing one set of penny-shaped fractures (the fractures are parallel with the y,z-plane).

$$C_{ijkl} = \frac{\rho a^2}{2} \int_{\Omega/2} \left[B_1(\alpha_{i1'}n_j + \alpha_{j1'}n_i)\beta_{1'k}\beta_{1'l} + B_2(\alpha_{i2'}n_j + \alpha_{j2'}n_i) \times \beta_{1'k}\beta_{2'l} + B_2(\alpha_{i3'}n_j + \alpha_{j3'}n_i)\beta_{1'k}\beta_{3'l} \right] d\Omega \quad (25)$$

Component C_{1111} is related to the elastic modulus, as follows:

$$
\begin{aligned}
C_{1111} &= \frac{\rho a^2}{2} \int_{\Omega/2} \left[B_1(\alpha_{11'}n_1 + \alpha_{11'}n_1)\beta_{1'1}\beta_{1'1} + B_2(\alpha_{12'}n_1 + \alpha_{12'}n_1)\beta_{1'1}\beta_{2'1} + B_2(\alpha_{13'}n_1 + \alpha_{13'}n_1)\beta_{1'1}\beta_{3'1} \right] d\Omega \\
&= \frac{\rho a^2}{2} \int_{\Omega/2} \left(2B_1 n_1 \alpha_{11'}\beta_{1'1}^2 + 2B_2 n_1 \alpha_{12'}\beta_{1'1}\beta_{2'1} + 2B_2 n_1 \alpha_{13'}\beta_{1'1}\beta_{3'1} \right) d\Omega \\
&= \rho a^2 \int_0^{\pi/2} \sin\theta\, d\theta \int_0^{2\pi} d\varphi \left(B_1 \sin^4\theta \cos^4\varphi + B_2 \sin^2\theta \cos^2\theta \cos^4\varphi + B_2 \sin^2\theta \sin^2\varphi \cos^2\varphi \right) \\
&= \rho \pi a^2 \left(\frac{2}{5} B_1 + \frac{4}{15} B_2 \right)
\end{aligned}
\quad (26)
$$

Submitting B_1 and B_2 into Eq. (26), the effective elastic modulus of randomly distributed penny-shaped fractures is obtained as

$$\frac{1}{E} = \frac{1}{E_0} + \frac{16\rho\pi(1-v_0^2)a^3}{80K_n(1-v_0^2)a + 15\pi E_0} + \frac{64\rho\pi(1-v_0^2)a^3}{480K_s(1-v_0^2)a + 45\pi E_0(2-v_0)} \quad (27)$$

For open fractures ($K_n = K_s = 0$), Eq. (27) confirms the result of Kemeny and Cook (1986), as follows:

Table 2. Parameters of intact rock and fractures

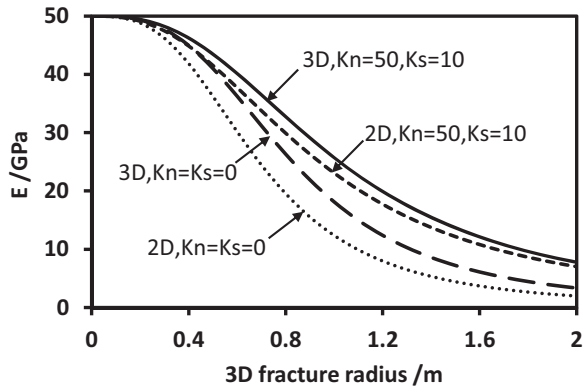| Property	Value
Elastic modulus (GPa)	50
Poisson's ratio	0.25
Fracture dip/dip angle (degrees)	90/90
Fracture normal stiffness (GPa/m)	50
Fracture shear stiffness (GPa/m)	10
Penny-shaped fracture density (m^3)	1
Penny-shaped fracture radius (m)	1
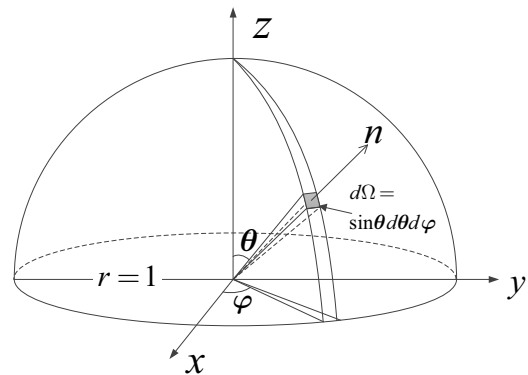
Fig. 4. Half-unit sphere to define the solid angle $d\Omega$.
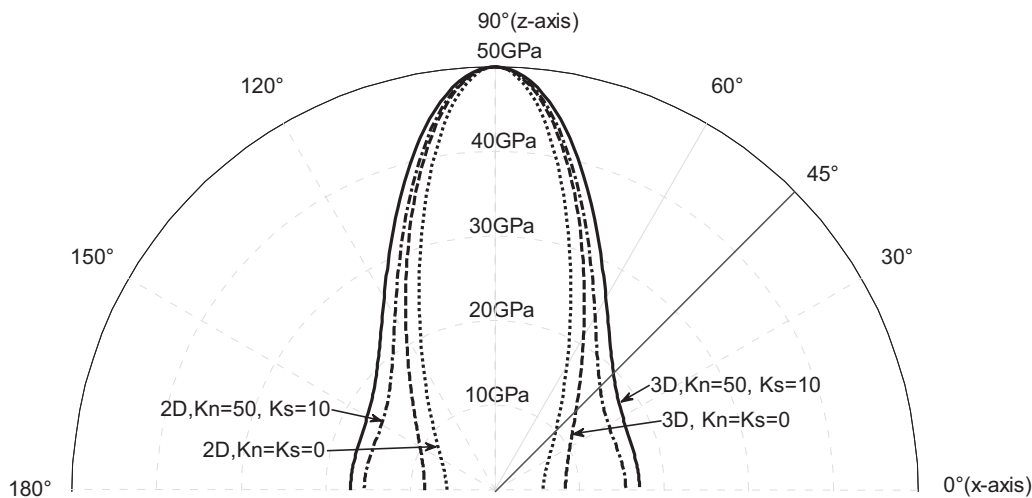
Fig. 3. Comparison of elastic moduli of rock mass containing one set of fractures.
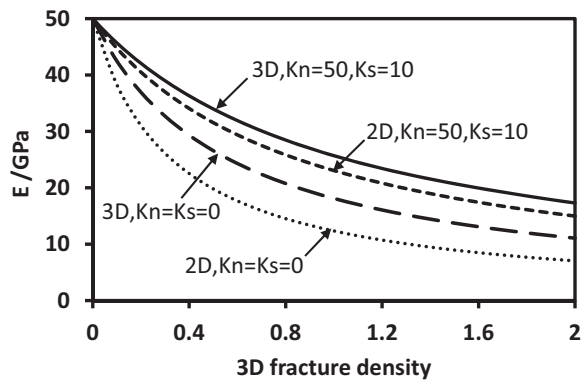
(a)

(b)

Fig. 5. Elastic moduli for rock mass containing randomly distributed penny-shaped fractures: (a) variation of equivalent elastic moduli with ρ ($a = 1$); and (b) variation of equivalent elastic moduli with a ($\rho = 1$).

$$\frac{1}{E} = \frac{1}{E_0} + \frac{16\rho a^3 \left(1 - v_0^2\right)\left(10 - 3v_0\right)}{45 E_0(2 - v_0)} \qquad (28)$$

The relationships between a 3D fracture network and the corresponding 2D trace maps were systematically analyzed by Berkowitz and Adler (1998). For randomly distributed penny-shaped fractures, the deduced 2D fracture density (ρ_{2D}) and average half-trace length ($\langle a_{2D}\rangle$) are

$$\rho_{2D} = \frac{\pi \rho a}{2} \qquad (29)$$

$$\langle a_{2D}\rangle = \frac{\pi a}{4} \qquad (30)$$

The elastic modulus of 2D fractured rock masses containing fracture stiffness is (Yang et al. 2016)

$$\frac{1}{E} = \frac{1}{E_0} + \frac{\rho_{2D}\pi a_{2D}^2}{4}\left(\frac{3}{K_n \pi a_{2D} + E_0} + \frac{1}{K_s \pi a_{2D} + E_0}\right) \qquad (31)$$

To estimate the compliance of fractured rock, a rock mass containing randomly distributed penny-shaped fractures is considered here, and the mechanical parameters of the materials were chosen from the previously studied case (Table 2). Figs. 5(a and b) present the variation of elastic moduli with fracture density ρ and fracture radius a, respectively. The models considering fracture stiffness predicted larger elastic moduli than the open-fracture models, and the 3D models predicted larger elastic

moduli than the corresponding 2D models. As presented in Fig. 5(a), the maximum decrease of the elastic moduli from 3D to 2D open fracture model was 36%, and it was 13% for the resistant-fracture model. As presented in Fig. 5(b), the maximum decreases were 40% and 11% for the open-fracture model and resistant-fracture model, respectively. These results imply that when the 2D outcrop trace map and 2D open-fracture model are used to estimate the equivalent elastic modulus of rock masses, the elastic modulus will be underestimated by 30–40% compared with the 3D model result. If fracture stiffness is considered, the difference between the 2D and 3D results will decrease. As fracture stiffness increases, the 2D result will gradually approach the 3D result. For the present study, the difference between 2D and 3D results was less than 15%.

Conclusions

1. In geotechnical engineering, the fracture fillings or rough fracture surfaces often resist deformation. In this study, the normal and shear stiffness of fractures were incorporated into the open-fracture model to account for the normal and shear resistance of fractures. The displacements of penny-shaped fractures incorporating fracture stiffness were derived. As fracture stiffness reduced to zero, the displacements reduced to the theoretic results of an open fracture.
2. The elastic compliance tensor of arbitrarily distributed fractures was derived based on the proposed fracture-displacement expressions. The compliance matrices of two special fracture distributions, the parallel and random distribution, were obtained. Using the parallel distribution result, the elastic compliance matrix of rock masses containing several sets of penny-shaped fractures can be estimated by summation of the compliance matrix of each fracture set in the global coordinate system.
3. By analyzing 3D fracture networks and corresponding 2D trace maps, the elastic moduli between 3D and 2D models were compared. The elastic moduli of open fractures were also studied to investigate the influence of fracture stiffness. The results show that 3D models predicted larger elastic moduli than the corresponding 2D models, and models considering fracture stiffness predicted larger elastic moduli than open-fracture models. The elastic moduli from 2D open-fracture models were underestimated by 30–40% relative to the 3D models. The difference in elastic moduli between 2D and 3D models was found to decrease with consideration of fracture stiffness. In the present study, the difference was less than 15%.
4. The simplified fracture model adopted in the present study does not consider the complexity of real fracture shapes (Zhang and Einstein 2010), the nonlinearity of fracture deformation behavior (Bandis et al. 1983), and the interaction between neighboring fractures (Kachanov 1993). The derived expressions will be improved in the future to estimate the compliance matrix of rock masses in the nonelastic range.

Notation

The following symbols are used in this paper:

A = area of penny-shaped fracture;
a = radius of penny-shaped fracture;
a_{2D} = half length of 2D fracture;
C_{ijkl} = components of elastic compliance tensor of fractures;
D_{ijkl} = components of elastic compliance tensor of rock mass;
d = spacing of parallel persistent fractures;
E = effective deformation modulus of fractured rock mass;
E_0 = Young's modulus of intact rock;
G_0 = shear modulus of intact rock;
K_n = fracture normal stiffness;
K_s = fracture shear stiffness;
M_{ijkl} = components of elastic compliance tensor of intact rock;
n_i, n_j = components of fracture normal vector;
r = distance from fracture center to a point in the fracture surface;
$\mathbf{S}$ = compliance matrix of fractures;
$\mathbf{T}$ = transformation matrix;
u, v = normal and shear displacement of fracture face;
$\bar{u}, \bar{v}$ = average normal and shear displacement of fracture face;
u_i, u_j = components of fracture displacement;
V = volume of the fractured body;
α, β = rotation matrix;
δ_i, δ_j = mean displacement jump of fracture;
ν_0 = Poisson's ratio of intact rock;
ρ = density of penny-shaped fractures, defined as the number of fracture central points per unit volume;
ρ_{2D} = density of 2D fractures, defined as the number of fracture central points per unit square;
σ_e = effective normal stress acting on fracture faces;
σ_k = normal stress acting on fracture due to fracture stiffness;
σ_n = resolved normal stress on fracture plane from far-field stress; and
τ_s = resolved shear stress on fracture plane from far-field stress.

References

Agharazi, A., C. D. Martin, and D. D. Tannant. 2012. "A three-dimensional equivalent continuum constitutive model for jointed rock masses containing up to three random joint sets." *Geomech. Geoeng.* 7 (4): 227–238. https://doi.org/10.1080/17486025.2012.714476.

Amadei, B., and R. E. Goodman. 1981. "A 3-D constitutive relation for fractured rock masses." In *Proc., Int. Symp. on the Mechanical Behavior of Structured Media*, 249–268. New York: Elsevier.

Bakulin, A., V. Grechka, and I. Tsvankin. 2000. "Estimation of fracture parameters from reflection seismic data—Part I: HTI model due to a single fracture set." *Geophys.* 65 (6): 1788–1802. https://doi.org/10.1190/1.1444863.

Bandis, S. C., A. C. Lumsden, and N. R. Barton. 1983. "Fundamentals of rock joint deformation." *Int. J. Rock Mech. Min. Sci. Geomech. Abstr.* 20 (6): 249–268. https://doi.org/10.1016/0148-9062(83)90595-8.

Barton, N. 2002. "Some new Q-value correlations to assist in site characterisation and tunnel design." *Int. J. Rock Mech. Min. Sci.* 39 (2): 185–216. https://doi.org/10.1016/S1365-1609(02)00011-4.

Berkowitz, B., and P. M. Adler. 1998. "Stereological analysis of fracture network structure in geological formations." *J. Geophys. Res. Solid Earth* 103 (B7): 15339–15360. https://doi.org/10.1029/98JB01072.

Berryman, J. G. 2007. "Seismic waves in rocks with fluids and fractures." *Geophys. J. Int.* 171 (2): 954–974. https://doi.org/10.1111/j.1365-246X.2007.03563.x.

Bieniawski, Z. T. 1978. "Determining rock mass deformability: Experience from case histories." *Int. J. Rock Mech. Min. Sci. Geomech. Abstr.* 15 (5): 237–247. https://doi.org/10.1016/0148-9062(78)90956-7.

Budiansky, B., and R. J. O'Connell. 1976. "Elastic moduli of a cracked solid." *Int. J. Solids Struct.* 12 (2): 81–97. https://doi.org/10.1016/0020-7683(76)90044-5.

Cai, M., and H. Horii. 1992. "A constitutive model of highly jointed rock masses." *Mech. Mater.* 13 (3): 217–246. https://doi.org/10.1016/0167-6636(92)90004-W.

Esmaieli, K., J. Hadjigeorgiou, and M. Grenon. 2010. "Estimating geometrical and mechanical REV based on synthetic rock mass models at Brunswick Mine." *Int. J. Rock Mech. Min. Sci.* 47 (6): 915–926. https://doi.org/10.1016/j.ijrmms.2010.05.010.

Farahmand, K., I. Vazaios, M. S. Diederichs, and N. Vlachopoulos. 2018. "Investigating the scale-dependency of the geometrical and mechanical properties of a moderately jointed rock using a synthetic rock mass (SRM) approach." *Comput. Geotech.* 95: 162–179. https://doi.org/10.1016/j.compgeo.2017.10.002.

Grechka, V. 2005. "Penny-shaped fractures revisited." *Stud. Geophys. Geod.* 49 (3): 365–381. https://doi.org/10.1007/s11200-005-0015-3.

Gross, D., and T. Seelig. 2006. *Fracture mechanics—With an introduction to micromechanics.* Berlin: Springer.

Gutierrez, M., and D. J. Youn. 2015. "Effects of fracture distribution and length scale on the equivalent continuum elastic compliance of fractured rock masses." *J. Rock Mech. Geotech. Eng.* 7 (6): 626–637. https://doi.org/10.1016/j.jrmge.2015.07.006.

Hall, F., and Y. Wang. 2012. "Seismic response of fractures by numerical simulation." *Geophys. J. Int.* 189 (1): 591–601. https://doi.org/10.1111/j.1365-246X.2012.05360.x.

Hoek, E., and M. S. Diederichs. 2006. "Empirical estimation of rock mass modulus." *Int. J. Rock Mech. Min. Sci.* 43 (2): 203–215. https://doi.org/10.1016/j.ijrmms.2005.06.005.

Horii, H., and S. Nemat-Nasser. 1983. "Overall moduli of solids with microcracks: Load-induced anisotropy." *J. Mech. Phys. Solids* 31 (2): 155–171. https://doi.org/10.1016/0022-5096(83)90048-0.

Hu, K. X., and Y. Huang. 1993. "Estimation of the elastic properties of fractured rock masses." *Int. J. Rock Mech. Min. Sci. Geomech. Abstr.* 30 (4): 381–394. https://doi.org/10.1016/0148-9062(93)91721-T.

Huang, T. H., C. S. Chang, and Z. Y. Yang. 1995. "Elastic moduli for fractured rock mass." *Rock Mech. Rock Eng.* 28 (3): 135–144. https://doi.org/10.1007/BF01020148.

Hudson, J. A. 1994. "Overall properties of a material with inclusions or cavities." *Geophys. J. Int.* 117 (2): 555–561. https://doi.org/10.1111/j.1365-246X.1994.tb03952.x.

Kachanov, M. 1993. "Elastic solids with many cracks and related problems." *Adv. Appl. Mech.* 30: 259–445. https://doi.org/10.1016/S0065-2156(08)70176-5.

Kemeny, J., and N. G. W. Cook. 1986. "Effective moduli, non-linear deformation and strength of a cracked elastic solid." *Int. J. Rock Mech. Min. Sci. Geomech. Abstr.* 23 (2): 107–118. https://doi.org/10.1016/0148-9062(86)90337-2.

Kulatilake, P. H. S. W., S. Wang, and O. Stephansson. 1993. "Effect of finite-size joints on the deformability of jointed rock in three dimensions." *Int. J. Rock Mech. Min. Sci. Geomech. Abstr.* 30 (5): 479–501. https://doi.org/10.1016/0148-9062(93)92216-D.

Li, C. 2001. "A method for graphically presenting the deformation modulus of jointed rock masses." *Rock Mech. Rock Eng.* 34 (1): 67–75. https://doi.org/10.1007/s006030170027.

Min, K. B., and L. Jing. 2003. "Numerical determination of the equivalent elastic compliance tensor for fractured rock masses using the distinct element method." *Int. J. Rock Mech. Min. Sci.* 40 (6): 795–816. https://doi.org/10.1016/S1365-1609(03)00038-8.

Oda, M., K. Suzuki, and T. Maeshibu. 1984. "Elastic compliance for rock-like materials with random cracks." *Soils Found.* 24 (3): 27–40. https://doi.org/10.3208/sandf1972.24.3_27.

Palmstrøm, A. 1996. "Characterizing rock masses by the RMi for use in practical rock engineering: Part 1: The development of the Rock Mass index (RMi)." *Tunnelling Underground Space Technol.* 11 (2): 175–188. https://doi.org/10.1016/0886-7798(96)00015-6.

Saenger, E. H., O. S. Krüger, and S. A. Shapiro. 2004. "Effective elastic properties of randomly fractured soils: 3D numerical experiments." *Geophys. Prospect.* 52 (3): 183–195. https://doi.org/10.1111/j.1365-2478.2004.00407.x.

Saxena, N., and G. Mavko. 2015. "Effects of fluid-shear resistance and squirt flow on velocity dispersion in rocks." *Geophys.* 80 (2): D99–D110. https://doi.org/10.1190/geo2014-0304.1.

Takekawa, J., H. Mikada, and T. N. Goto. 2014. "Numerical simulation using a Hamiltonian particle method for effective elastic properties in cracked media." *Explor. Geophys.* 45 (2): 116–124. https://doi.org/10.1071/EG13098.

Wang, T. T., and T. H. Huang. 2009. "A constitutive model for the deformation of a rock mass containing sets of ubiquitous joints." *Int. J. Rock Mech. Min. Sci.* 46 (3): 521–530. https://doi.org/10.1016/j.ijrmms.2008.09.011.

Yang, J. P., W. Z. Chen, Y. H. Dai, and H. D. Yu. 2014. "Numerical determination of elastic compliance tensor of fractured rock masses by finite element modeling." *Int. J. Rock Mech. Min. Sci.* 70: 474–482. https://doi.org/10.1016/j.ijrmms.2014.06.007.

Yang, J. P., W. Z. Chen, G. J. Wu, and D. S. Yang. 2018. "Analytical estimation of the equivalent elastic compliance tensor for fractured rock masses." *Int. J. Geomech.* 18 (1): 04017126. https://doi.org/10.1061/(ASCE)GM.1943-5622.0001035.

Yang, J. P., W. Z. Chen, D. S. Yang, and H. M. Tian. 2016. "Estimation of elastic moduli of non-persistent fractured rock masses." *Rock Mech. Rock Eng.* 49 (5): 1977–1983. https://doi.org/10.1007/s00603-015-0806-y.

Zhang, L., and H. H. Einstein. 2004. "Using RQD to estimate the deformation modulus of rock masses." *Int. J. Rock Mech. Min. Sci.* 41 (2): 337–341. https://doi.org/10.1016/S1365-1609(03)00100-X.

Zhang, L., and H. H. Einstein. 2010. "The planar shape of rock joints." *Rock Mech. Rock Eng.* 43 (1): 55–68. https://doi.org/10.1007/s00603-009-0054-0.